Ab Initio Classical Trajectory Calculations of Acetylene Dication Dissociation

Xiaosong Li and H. Bernhard Schlegel*

Department of Chemistry, Wayne State University, Detroit, Michigan 48202

Received: August 28, 2003; In Final Form: November 12, 2003

Fragmentation of the acetylene dication on the $^3\Sigma_g^-$ surface has been studied by ab initio direct classical trajectory calculations at the B3LYP/6-31G(d) level of theory. The $C_2H_2^{2+} \rightarrow 2CH^+$ channel has a very small probability due to a high barrier. Though the barrier height for the decarbonation channel, $C_2H_2^{2+} \rightarrow H_2CC^{2+} \rightarrow H_2C^+ + C^+$, is much less than the available energy, this process was not observed in the simulation, possibly because of the two-step nature of the mechanism. The direct deprotonation channel, $C_2H_2^{2+} \rightarrow HCC^+ + H^+$, is the most abundant path. In addition to the direct mechanism, two other indirect deprotonation channels were observed. In our simulation, about 11−14% of the trajectories first went into the H_2CC^{2+} potential valley, but did not have enough energy in the CC stretching mode to dissociate into $H_2C^+ + C^+$. Strong coupling between the CH stretching and CCH bending eventually led one of the protons to depart from the molecule. Part of the indirect deprotonation was from the H_2CC^{2+} potential valley, while the rest was the result of recrossing into the $HCCH^{2+}$ potential valley.

Introduction

The acetylene dication ($C_2H_2^{2+}$) is one of the smallest stable polyatomic dications. It has been investigated extensively by both experiments[1−12] and theoretical caculations.[9,12−17] Experiments using classical mass spectrometry techniques[2,3] and photoelectron−photoion−photoion coincidence (PEPIPICO) spectroscopy[9,10] at 30.4 nm found three two-body dissociation channels:

$$C_2H_2^{2+} \rightarrow C_2H^+ + H^+ \quad (1)$$

$$\rightarrow CH_2^+ + C^+ \quad (2)$$

$$\rightarrow CH^+ + CH^+ \quad (3)$$

In the 25.6 nm photoionization experiment using the PEPIPICO technique,[11] the dissociative double ionization of the neutral C_2H_2 leads to three additional three-body fragmentation channels:

$$C_2H_2^{2+} \rightarrow C_2^+ + H + H^+ \quad (4)$$

$$\rightarrow C^+ + H + CH^+ \quad (5)$$

$$\rightarrow C + H^+ + CH^+ \quad (6)$$

Thissen and co-workers measured the branching ratio for channels 1 and 3 to be 57% and 38%, respectively.[11] Experimental cross-sections indicate that the thresholds are 34.0 ± 0.2, 34.0 ± 0.2, and 34.5 ± 0.2 eV above C_2H_2 for two-body fragmentation reactions 1−3 and 38.0 ± 0.4, 38.0 ± 0.4, and 40.0 ± 0.4 for the three-body fragmentation reactions 4−6.

It is well-known that removing two π electrons from the neutral acetylene leads to the three lowest lying states of $C_2H_2^{2+}$, $^3\Sigma_g^-$, $^1\Delta_g$, and $^1\Sigma_g^+$.[11−19] By comparing with experimental thresholds, theoretical calculations confirm that channel 1 is the most probable on the ground state ($^3\Sigma_g^-$) of $C_2H_2^{2+}$,[15,19] while channel 3 takes place mainly on the $^1\Sigma_g^+$ surface through a bent transition state.[19] Channel 2, which involves acetylene dication isomerization to vinylidene dication H_2CC^{2+}, followed by decarbonation, is considered to proceed on both the triplet and singlet states because activation barriers are very close to each other on these two surfaces.[19]

The experimentally observed fragments come from a combination of different surfaces. It is not possible to determine the branching ratio on a single surface when several electronic states are accessible under the experimental conditions. In this paper, we present direct ab intio trajectory calculations as a theoretical approach to study the branching ratios of the acetylene dication dissociation on the $^3\Sigma_g^-$ surface. In this approach, trajectories are computed "on the fly" from electronic structure calculations, without first fitting a global analytical potential energy surface. Whenever energies, gradients, or Hessians are needed for the trajectory integration, they are computed directly by molecular orbital methods. For a review of direct molecular dynamics calculations see ref 20.

Method

We chose to simulate reactions on the ground-state surface ($^3\Sigma_g^-$) of $C_2H_2^{2+}$. The development version of the GAUSSIAN series of programs was used to carry out all computations in the present study.[21] The geometries of the ground-state acetylene dication and its transition states were optimized at the HF/6-31G(d), B3LYP/6-31G(d), and QCISD/6-311G(d,p) levels of theory. The complete basis set extrapolation method with the atomic pair natural orbital basis set (CBS-APNO)[22] was used to compute accurate heats of reaction and barrier heights. Trajectories were computed at the B3LYP/6-31G(d) level of theory since spin contamination is too large at the MP2 level of theory.

The initial conditions were chosen to simulate a microcanonical ensemble of harmonic oscillators.[23] The available energy E_{tot} was distributed among the six vibrational normal modes. For a specific vibrational mode with a given vibrational energy, the initial phase was chosen randomly. Since the actual potential energy surface is not strictly harmonic, the initial vibrational coordinates and momenta generated by this procedure

10.1021/jp0365662 CCC: $27.50
Published on Web 12/20/2003

TABLE 1: Optimized Geometries of the Ground-State $C_2H_2^{2+}$ (Å)

	H−C−C−H		H−C−C−H^{2+}	
	R_{C-H}	R_{C-C}	R_{C-H}	R_{C-C}
HF/6-31G(d)[a]	1.057	1.185	1.113	1.308
B3LYP/6-31G(d)	1.067	1.205	1.130	1.341
QCISD/6-311G(d,p)	1.066	1.210	1.130	1.339
CASSCF(8,10)/TZP[b]	1.062	1.216	1.137	1.344
experiment[c]	1.060	1.203		

[a] Reference 15. [b] Reference 19. [c] Reference 30.

were scaled to yield the desired vibrational energy.[24] Because of the shape of the potential energy surface, this scaling procedure did not converge in ~20% of the cases and these initial points were rejected. The total angular momentum was set to zero. For each energy, about 200 trajectories were integrated. More extensive sampling of the initial conditions would have been desirable but was limited by practical considerations.

Trajectories were integrated for each of three different initial energies, E_{tot} = 130, 150, and 170 kcal/mol. For the highest initial energy, this corresponds to an average of 20−30 kcal/mol in each of the normal modes. The trajectories were calculated directly from the electronic structure computations without first fitting a global potential energy surface. A Hessian-based predictor−corrector method with updating was employed to integrate the trajectories.[25,26] The Hessian was updated for five steps before being recalculated analytically. In this method, the step size is controlled by a trust radius distance in mass-weighted coordinates rather than a constant time interval. A step size of 0.25 amu$^{1/2}$ bohr is used in all of the trajectory calculations. A quadratically convergent SCF algorithm[27] was used to avoid SCF convergence problems during the trajectory integrations. Trajectories were stopped when the products were ~8 bohr apart or the gradient of the potential between product molecules was less than 1×10^{-5} hartree/bohr. The total energy and total angular momentum were conserved to 10^{-7} hartree and better than $10^{-8}\hbar$, respectively. The mass-weighted steepest descent reaction paths were calculated using the method of Gonzalez and Schlegel.[28,29]

Results and Discussions

Structures and Energetics. Optimized equilibrium geometries and vibrational frequencies of ground-state $^3\Sigma_g^-$ $C_2H_2^{2+}$ are listed in Tables 1 and 2, respectively. The energetics are listed in Table 3 and shown in Figure 1. The geometrical parameters and harmonic frequencies at the B3LYP/6-31G(d), QCISD/6-311G(d,p), and CASSCF(8,10)/TZP levels of theory are in very good agreement with each other. However, computations at HF/6-31G(d) differ rather significantly from those calculated using higher levels of theory; the disagreement is due to a lack of electron correlation, which can be very important for correctly predicting structures and energetics of π systems. The C−C distance in $C_2H_2^{2+}$, 1.34 Å, is much longer than that in the neutral and the monocation (1.20 Å for C_2H_4 and 1.23 Å for $C_2H_2^+$), because removing two π electrons leads to a triplet state with a formal CC bond order of 2. There is also a significant lengthening of the CH bond. Accompanying the CC bond weakening, there is a large red shift in the CC bond stretching frequency in $C_2H_2^{2+}$ (1580 cm^{-1} compare to 1977 cm^{-1} in the neutral acetylene[19]).

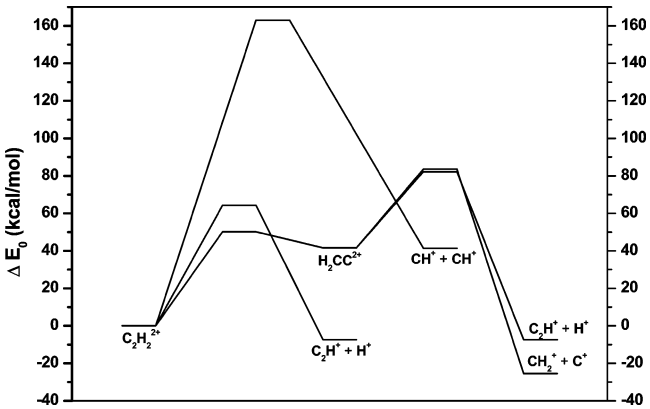

Figure 1. Energy profile for two-body dissociations of $C_2H_2^{2+}$ on the ground-state surface computed at the CBS-APNO level of theory.

a. $C_2H_2^{2+}(^3\Sigma_g^-) \rightarrow C_2H^+(^3\Sigma^-) + H^+$. The direct deprotonation reaction of the acetylene dication on the ground-state surface ($^3\Sigma_g^-$) produces C_2H^+ and a proton. Table 3 lists calculated energetics for the various acetylene dication two-body dissociation channels. For the direct deprotonation channel, our best computational method, CBS-APNO, predicts a barrier height of 64.3 kcal/mol (34.5 eV above the neutral acetylene after ZPE correction), which is in good agreement with the experimental threshold of 34.0 ± 0.2 eV. All methods considered in this work are consistent with each other for the barrier height of the direct deprotonation reaction. Except for CIPSI//CASSCF(8,10)/TZP, all of the methods show that channel 1 is slightly exothermic after zero-point energy correction. This is because the C−H bond energy is balanced by the decrease in Coulomb repulsion. The optimized transition structure for direct deprotonation is listed in Table 4, along with the transition structure for the deprotonation of vinylidene dication. For $HCCH^{2+}$ deprotonation, the C−H_a bond length varies significantly from one method to the other. The B3LYP/6-31G(d) method predicts a rather late transition state, while in the HF/6-31G(d)-optimized TS the C−H_a distance is about 0.17 Å shorter. The potential surface is very flat around the transition states; even relatively large changes of geometry along the transition vector do not affect the barrier height significantly. There is less variability in the transition-state geometry for vinylidene dication deprotonation. In general, geometries and energetics at B3LYP/6-31G(d) are consistent with higher levels of theory. Again, disagreements in geometries with correlation methods disfavor the use of the HF/6-31G(d) method in trajectory computations.

b. $C_2H_2^{2+}(^3\Sigma_g^-) \rightarrow 2CH^+(^3\Pi)$. Homogeneous C−C bond dissociation on the ground-state surface produces CH^+ fragments in their first excited state ($^3\Pi$). The HF/6-31G(d) barrier is too high, but the B3LYP/6-31G(d) barrier height of 128.3 kcal/

TABLE 2: Harmonic Frequencies[a] of the Ground-State $C_2H_2^{2+}$ (cm^{-1})

	HF/6-31G(d)	B3LYP/6-311G(d,p)	QCISD/6-311G(d,p)	CASSCF(8,10)/TZP[b]
CCH sym bend	690	639	682	646
CCH asym bend	727	646	659	652
CC stretch	1770	1579	1580	1546
CH sym stretch	3010	2826	2943	2753
CH asym stretch	3141	2944	2822	2863

[a] Unscaled harmonic frequencies. [b] Reference 19.

TABLE 3: Energetics for $C_2H_2^{2+}$ ($^3\Sigma_g^-$) Dissociation (kcal/mol)

	ΔE^c	ΔE_0^d	$\Delta E^{\ddagger c}$	$\Delta E_0^{\ddagger d}$
$C_2H_2^{2+}(^3\Sigma_g^-) \rightarrow C_2H^+(^3\Sigma^-) + H^+$				
HF/6-31G(d)	0.8	−4.9	72.6	66.7
B3LYP/6-31G(d)	−0.6	−2.0	67.3	61.6
MP4SDQ/6-31G(d,p)//HF/6-31G(d)[a]	−0.6	−6.4	71.3	65.4
CIPSI//CASSCF(8,10)/TZP[b]	7.9		67.0	61.3
CBS-APNO	−2.4	−7.4	69.4	64.3
$C_2H_2^{2+}(^3\Sigma_g^-) \rightarrow CH^+(^3\Pi) + CH^+(^3\Pi)$				
HF/6-31G(d)	−4.6	−11.1	195.6	189.5
B3LYP/6-31G(d)	52.9	46.4	133.5	128.3
CIPSI//CASSCF(8,10)/TZP[b]	38.9		135.0	
CBS-APNO	47.4	41.4	163.3	158.8[e]
$C_2H_2^{2+}(^3\Sigma_g^-) \rightarrow H_2CC^{2+}(^3B_1)$				
HF/6-31G(d)	33.2	33.0	62.0	59.2
B3LYP/6-31G(d)	41.9	40.9	59.9	57.1
CIPSI//CASSCF(8,10)/TZP[b]	36.8		51.7	50.8
CBS-APNO	41.8	41.6	52.6	50.2
$H_2CC^{2+}(^3B_1) \rightarrow H_2C^+(^2A_1) + C^+(^2P)$				
HF/6-31G(d)	−82.5	−86.5	60.7	58.8
B3LYP/6-31G(d)	−55.0	−57.3	46.0	44.7
CIPSI//CASSCF(8,10)/TZP[b]	−69.5		40.3	39.0
CBS-APNO	−63.5	−67.0	43.7	42.0
$H_2CC^{2+}(^3B_1) \rightarrow HCC^+(^3\Sigma^-) + H^+$				
B3LYP/6-31G(d)	−42.6	−42.9	43.3	39.2
CBS-APNO	−44.2	−49.0	45.3	40.6

[a] Reference 15. [b] Reference 19. [c] Without ZPE. [d] With ZPE. [e] ZPE at QCISD/6-311G(d,p) without scaling.

mol (after ZPE correction) is in good agreement with CIPSI estimations by Duflot and co-workers.[19] Because several potential surfaces are very close to each other at the saddle point, the QCISD calculations encounter convergence difficulties. The maximum in the relaxed potential surface scan yielded an approximate transition structure (see Table 5). The barrier height was estimated from CBS-APNO calculations at points along the QCISD relaxed scan and was found to be ca. 30 kcal/mol higher than the value obtained by Duflot. However, the transition state on the ground-state surface of the acetylene dication is not the lowest lying saddle point to produce CH^+ fragments (see ref 19 for a detailed discussion). Nevertheless, since our goal is to determine the branching ratio arising from a single surface, we focus on reactions only on the ground-state surface.

c. $C_2H_2^{2+}(^3\Sigma_g^-) \rightarrow H_2CC^{2+}(^3B_1) \rightarrow H_2C^+(^2A_1) + C^+(^2P)$. This reaction proceeds by a two-step mechanism. In the first step, acetylene dication undergoes an in-plane 1,2-hydrogen-shift rearrangement, leading to the $^3B_1$ state of the vinylidene dication H_2CC^{2+}. At the transition state of the isomerization process, the CH_a bond length remains intact (Table 6); the CC bond is slightly shorter and the CH_b bond is longer than those in the equilibrium $C_2H_2^{2+}$ structure (Table 1). When hydrogen shifts from one carbon to the other, it forms a three-center, three-electron bridging bond (C···H_b···C bond), which subsequently strengthens the CC bond and shortens the CH_b bond. The barrier height for this isomerization reaction is 52.6 kcal/mol at the CBS-APNO level of theory (Table 3). The barrier calculated at the B3LYP level is ca. 7 kcal/mol higher, which may reduce the number of trajectories passing through H_2CC^{2+} as an intermediate. The vinylidene dication intermediate is a $^3B_1$ structure, lying 41.8 kcal/mol above the ground-state acetylene dication. The CC bond in the vinylidene dication is about 0.05 Å longer than that in the equilibrium $C_2H_2^{2+}$ due to the loss of one π-bonding electron. The second step involves dissociation of the vinylidene dication into H_2C^+ and C^+ fragments. In the equilibrium structure of $H_2C_aC_b^{2+}$, C_a and C_b form one doubly occupied in-plane σ bond and one singly occupied out-of-plane π bond; in addition, C_b has a singly occupied in-plane p orbital. When we consider the breaking of the CC bond, analysis of the molecular orbitals shows that C_a takes the electron from the π orbital, leaving C_b with the electron pair from the σ bond; this dissociation scheme leads to a $^2B_1$ electron configuration for the H_2C^+ fragment and ground-state ^2P for the C^+ product. However, the linear $^2B_1$ state of the H_2C^+ product is not the ground state; it has a large imaginary frequency, and optimization leads to the more stable $^2A_1$ structure. We choose the $^2A_1$ state of the H_2C^+ product as our reference state when calculating energetics. The transition state has $^3B_1$ symmetry; the geometries obtained at the HF and QCISD levels of theory have larger $\angle HC_aC_b$ angles and longer CH and CC bonds than those at the CASSCF and B3LYP levels. Orbital analysis indicates that, at the saddle point, the σ bond has already broken completely, leaving an electron pair in C_b's 2s orbital. In the case of HF and QCISD, the π bond breaking is almost completed, resulting in the transition state resembling the product. By contrast, in the transition states calculated at the CASSCF and B3LYP levels of theory, the π bond is just starting to break.

Dynamics. $C_2H_2^{2+}$ dissociation via the deprotonation channel is the most abundant in experiment. Examining barrier heights of reactions of interest in Table 3, one would conclude that the isomerization reaction of vinylidene dication is most probable. However, the decarbonation step after isomerization requires an additional 43.7 kcal/mol to overcome the barrier, which is 85.5 kcal/mol above the equilibrium $C_2H_2^{2+}$. As can be seen from Figure 1, this makes subsequent dissociation to $CH_2^+ + C^+$ unfavorable, so that recrossing back to the reactant domi-

TABLE 4: Geometrical Parameters for $HCCH^{2+} \rightarrow HCC^+ + H^+$ and $H_2CC^{2+} \rightarrow HCC^+ + H^+$ (Å)

Method	$H_a\cdots C{-}C{-}H_b^{2+}$			→ H^+ +	$C{-}C{-}H_b^+$	
	$R_{C\text{-}Ha}$	$R_{C\text{-}C}$	$R_{C\text{-}Hb}$		$R_{C\text{-}C}$	$R_{C\text{-}H}$
HF/6-31G(d)	2.707	1.331	1.091		1.345	1.080
B3LYP/6-31G(d)	2.881	1.366	1.109		1.381	1.096
QCISD/6-311G(d,p)	2.717	1.365	1.107		1.379	1.095
CASSCF(8,10)/TZP[a]	2.750	1.368	1.115		1.382	1.078

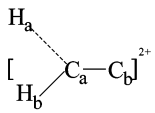

	$R_{C\text{-}Ha}$	$R_{C\text{-}C}$	$R_{C\text{-}Hb}$	$\angle H_aC_aC_l$	$\angle H_bC_aC_l$
B3LYP/6-31G(d)	2.508	1.298	1.111	102.1	156.1
QCISD/6-311G(d,p)	2.469	1.300	1.108	102.5	152.2

[a] Reference 19.

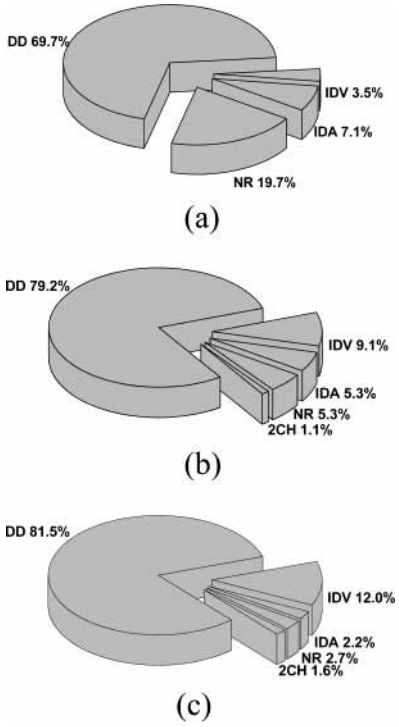

Figure 2. Branching ratios for $C_2H_2^{2+}$ dissociation: (a) E_{tot} = 130 kcal/mol, (b) E_{tot} = 150 kcal/mol, and (c) E_{tot} = 170 kcal/mol. DD = direct deprotonation, IDV = indirect deprotonation via vinylidene dication, IDA = indirect deprotonation via acetylene dication, and NR = no reaction, 2CH = $C_2H_2^{2+} \rightarrow 2CH^+$.

TABLE 5: Geometrical Parameters for $C_2H_2^{2+} \rightarrow 2CH^+$ (Å)

	$H_a-C\cdots C-H_b^{2+} \rightarrow 2C-H^+$		
method	R_{C-H}	R_{C-C}	R_{C-H}
HF/6-31G(d)	1.132	4.886	1.102
B3LYP/6-31G(d)	1.153	3.456	1.140
QCISD/6-311G(d,p)[a]	1.170	3.021	1.139
CASSCF(8,10)/TZP[b]			1.135

[a] TS obtained from a relaxed potential surface scan along the CC bond. [b] Reference 19.

nates, leading to other channels and much longer reaction times. Furthermore, the two-step decarbonation reaction requires appropriate excitation in both the CCH bending and the C−C stretching modes, making this pathway less probable. By comparison, the deprotonation requires only modest excitation in the CH stretching mode and is a one-step reaction. Therefore, channel 1 should be a faster and favorable reaction. Our results with different available energies confirmed this rationalization.

Figure 2 shows branching ratios obtained from three sets of trajectories. The decarbonation channel was not seen in the simulation, suggesting that necessary energy redistribution in vinylidene needed for C−C dissociation on the triplet surface

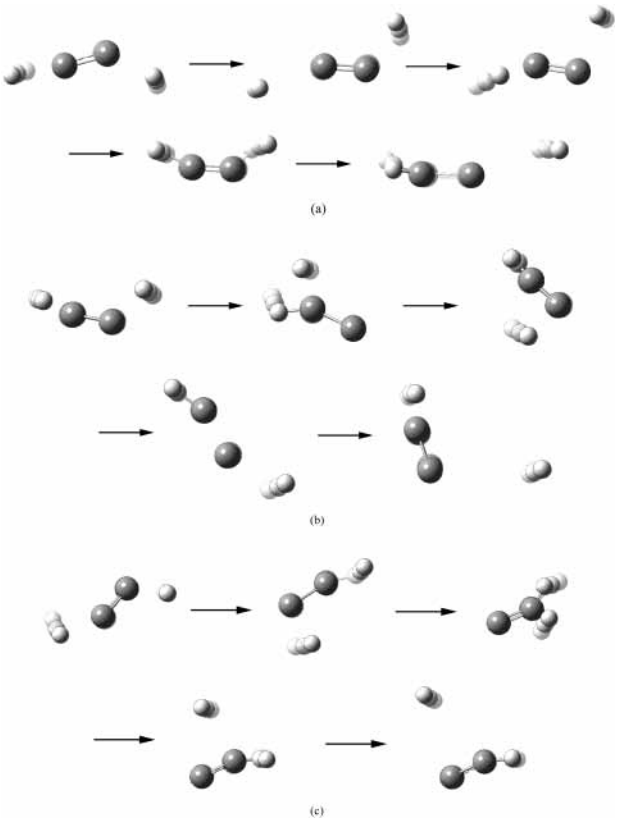

Figure 3. Snapshots along typical trajectories for (a) DD, $HCCH^{2+} \rightarrow HCC^+ + H^+$, (b) IDA, $HCCH^{2+} \rightarrow H_2CC^{2+} \rightarrow HCCH^{2+} \rightarrow HCC^+ + H^+$, and (c) IDV, $HCCH^{2+} \rightarrow H_2CC^{2+} \rightarrow HCC^+ + H^+$.

may be slower than isomerization or deprotonation of vinylidene. The percentage of the nonreactive trajectories decreases as the total available energy increases. The $C_2H_2^{2+} \rightarrow 2CH^+$ channel has a very low probability because it has a very high barrier. Duflot attributed the large branching ratio in experiments to dissociation on the $^1\Sigma_g^+$ surface through a bent transition state.[19] This prediction is very reasonable considering a much lower barrier height calculated on the $^1\Sigma_g^+$ surface.

The deprotonation reaction has the highest probability for the three simulations we have run. By inspecting the trajectories, we find there are three mechanisms that lead to deprotonation as shown in Figure 3. The first case is the well-studied direct deprotonation (DD) channel, $HCCH^{2+} \rightarrow HCC^+ + H^+$. In the second and third cases, vibrationally excited acetylene first proceeds into the H_2CC^{2+} potential valley. In one case, one of the CH stretches gets excited by coupling with other modes, and subsequently, this proton is detached from the H_2CC^{2+} molecule. The $H_2CC^{2+} \rightarrow HCC^+ + H^+$ reaction has a barrier height of 39.2 kcal/mol at the B3LYP/6-31G(d) level of theory, which is slightly lower than that of the decarbonation channel. This mechanism is denoted as IDV (indirect deprotonation via

TABLE 6: Geometrical Parameters for $C_2H_2^{2+} \rightarrow H_2CC^{2+} \rightarrow CH_2^+ + C^+$ (Å, deg)

Method	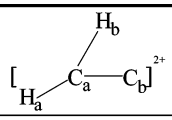					→	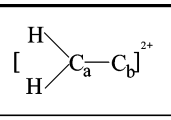			→	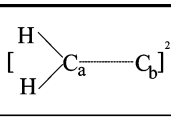			→	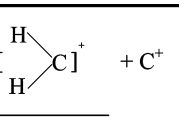		+ C^+
	R_{Ca-Ha}	R_{Ca-Hb}	R_{C-C}	$\angle H_aC_aC_b$	$\angle H_bC_aC_b$		R_{Ca-H}	R_{C-C}	$\angle HC_aH$		R_{Ca-H}	R_{C-C}	$\angle HC_aH$		R_{C-H}	$\angle HCH$	
HF/6-31G(d)	1.116	1.371	1.276	177.4	61.9		1.113	1.409	123.2		1.095	1.968	160.5		1.080	138.7	
B3LYP/6-31G(d)	1.136	1.384	1.302	175.5	64.1		1.149	1.381	121.0		1.119	2.417	146.6		1.099	140.3	
QCISD/6-311G(d,p)	1.134	1.385	1.310	175.8	64.0		1.143	1.402	123.9		1.111	2.291	168.0		1.099	139.9	
CASSCF(8,10)/TZP[a]	1.140	1.403	1.313	176.7	63.7		1.152	1.398	122.5		1.124	2.391	143.7		1.105	137.0	

[a] Reference 19.

vinylidene). In the other case, the molecular system recrosses the isomerization transition state back to the $HCCH^{2+}$ potential valley. During such recrossing, one of the protons gains enough energy from vibrational coupling with other modes, and finally dissociates from acetylene. This is denoted IDA (indirect deprotonation via acetylene). In a few trajectories, the molecule experienced more than one isomerization recrossing, but still ends up producing a proton and HCC^+. The DD mechanism has the shortest reaction time, followed by the IDV and IDA channels. For all the channels observed in this study, reaction time decreases as the total available energy increases.

Conclusion

The dissociation of acetylene dication on the $^3\Sigma_g^-$ surface has been studied using ab initio molecular dynamics calculations. The geometric parameters of the reactant and products are in good agreement with earlier calculations. The potential energy surfaces at the transition states are very flat for the deprotonation channels and the $2CH^+$ channel, leading to relatively large deviations in the geometry from one method to another. The barrier height for the direct deprotonation reaction was found lowest, and is in good agreement with experiments.

Trajectory calculations at the B3LYP/6-311G(d,p) level of theory were started from ensembles with three different available energies, 130, 150, and 170 kcal/mol. Notwithstanding the usual caveats associated with classical trajectory calculations (e.g., lack of tunneling, etc.) and the simplifications made in selecting the initial conditions (e.g., lack of rotational energy, etc.), deprotonation is found to be the dominant process on the ground-state triplet surface. The $2CH^+$ pathway has a very small probability ground-state triplet surface due to a high barrier. The decarbonation channel, $CH_2^+ + C^+$, is not seen in the present simulation, possibly due to a dynamical bottleneck. The DD channel has the highest probability and the shortest reaction time. In addition to the direct deprotonation of acetylene dication, two new deprotonation pathways are found, IDV and IDA. As the total available energy increases, DD and IDV become more favorable and the reaction times decrease. No triple dissociations were seen in the present simulations.

Acknowledgment. This work was supported by a grant from the National Science Foundation (CHE 0131157). We thank the National Center for Supercomputing Applications and the ISC at Wayne State University for computer time.

References and Notes

(1) Beynon, J. H.; Mathias, A.; Williams, A. E. *Org. Mass Spectrom.* **1971**, *5*, 303.

(2) Ast, T.; Beynon, J. H.; Cooks, R. G. *Org. Mass Spectrom.* **1972**, *6*, 741.

(3) Mathur, B. P.; Abbey, L. E.; Burgess, E. M.; Moran, T. F. *Org. Mass Spectrom.* **1980**, *15*, 312.

(4) Jones, B. E.; Abbey, L. E.; Chatham, H. L.; Hanner, A. W.; Teleshefsky, L. A.; Burgess, E. M.; Moran, T. F. *Org. Mass Spectrom.* **1982**, *17*, 10.

(5) Rye, R. R.; Madey, T. E.; Houston, J. E.; Holloway, P. H. *J. Chem. Phys.* **1978**, *69*, 1504.

(6) Thompson, M.; Hewitt, P. A.; Wooliscroft, D. S. *Anal. Chem.* **1976**, *48*, 1336.

(7) Appell, J.; Durup, J.; Fehsenfeld, F. C.; Fournier, P. *J. Phys. B* **1974**, *7*, 406.

(8) Andrews, S. R.; Harris, F. M.; Parry, D. E. *Chem. Phys.* **1992**, *166*, 69.

(9) Eland, J. H. D.; Wort, F. S.; Lablanquie, P.; Nenner, I. *Z. Phys. D: At., Mol. Clusters* **1986**, *4*, 31.

(10) Eland, J. H. D.; Price, S. D.; Cheney, J. C.; Lablanquie, P.; Nenner, I.; Fournier, P. G. *Philos. Trans. R. Soc. London, Ser. A* **1988**, *324*, 247.

(11) Thissen, R.; Delwiche, J.; Robbe, J. M.; Duflot, D.; Flament, J. P.; Eland, J. H. D. *J. Chem. Phys.* **1993**, *99*, 6590.

(12) Burdick, G. W.; Shields, G. C.; Appling, J. R.; Moran, T. F. *Int. J. Mass Spectrom. Ion Processes* **1985**, *64*, 315.

(13) Shields, G. C.; Moran, T. F. *Theor. Chim. Acta* **1986**, *69*, 147.

(14) Appling, J. R.; Moran, T. F. *Chem. Phys. Lett.* **1985**, *118*, 188.

(15) Pople, J. A.; Frisch, M. J.; Raghavachari, K.; Schleyer, P. V. *J. Comput. Chem.* **1982**, *3*, 468.

(16) Ohrendorf, E. M. L.; Tarantelli, F.; Cederbaum, L. S. *J. Chem. Phys.* **1990**, *92*, 2984.

(17) Liegener, C. M. *Chem. Phys.* **1985**, *92*, 97.

(18) Hanner, A. W.; Abbey, L. E.; Bostwick, D. E.; Burgess, E. M.; Moran, T. F. *Org. Mass Spectrom.* **1982**, *17*, 19.

(19) Duflot, D.; Robbe, J. M.; Flament, J. P. *J. Chem. Phys.* **1995**, *102*, 355.

(20) Bolton, K.; Hase, W. L.; Peslherbe, G. H. In *Modern Methods for Multidimensional Dynamics Computation in Chemistry*; Thompson, D. L., Ed.; World Scientific: Singapore, 1998.

(21) Frisch, M. J.; Trucks, G. W.; Schlegel, H. B.; Scuseria, G. E.; Robb, M. A.; Cheeseman, J. R.; Zakrzewski, V. G.; Montgomery, J. A.; Stratmann, R. E.; Burant, J. C.; Dapprich, S.; Millam, J. M.; Daniels, A. D.; Kudin, K. N.; Strain, M. C.; Farkas, O.; Tomasi, J.; Barone, V.; Cossi, M.; Cammi, R.; Mennucci, B.; Pomelli, C.; Adamo, C.; Clifford, S.; Ochterski, J.; Petersson, G. A.; Ayala, P. Y.; Cui, Q.; Morokuma, K.; Malick, D. K.; Rabuck, A. D.; Raghavachari, K.; Foresman, J. B.; Cioslowski, J.; Ortiz, J. V.; Stefanov, B. B.; Liu, G.; Liashenko, A.; Piskorz, P.; Komaromi, I.; Gomperts, R.; Martin, R. L.; Fox, D. J.; Keith, T.; Al-Laham, M. A.; Peng, C. Y.; Nanayakkara, A.; Gonzalez, C.; Challacombe, M.; Gill, P. M. W.; Johnson, B. G.; Chen, W.; Wong, M. W.; Andres, J. L.; Head-Gordon, M.; Replogle, E. S.; Pople, J. A. *Gaussian 01*, development version; Gaussian, Inc.: Pittsburgh, PA, 2002.

(22) Montgomery, J. A.; Ochterski, J. W.; Petersson, G. A. *J. Chem. Phys.* **1994**, *101*, 5900.

(23) Hase, W. L.; Buckowski, D. G. *Chem. Phys. Lett.* **1980**, *74*, 284.

(24) Hase, W. L. In *Encyclopedia of Computational Chemistry*; Schleyer, P. v. R., Allinger, N. L., Clark, T., Gasteiger, J., Kollman, P. A., Schaefer, H. F., III, Schreiner, P. R., Eds.; Wiley: New York, 1998; p 402.

(25) Millam, J. M.; Bakken, V.; Chen, W.; Hase, W. L.; Schlegel, H. B. *J. Chem. Phys.* **1999**, *111*, 3800.

(26) Bakken, V.; Millam, J. M.; Schlegel, H. B. *J. Chem. Phys.* **1999**, *111*, 8773.

(27) Bacskay, G. B. *Chem. Phys.* **1981**, *61*, 385.

(28) Gonzalez, C.; Schlegel, H. B. *J. Chem. Phys.* **1989**, *90*, 2154.

(29) Gonzalez, C.; Schlegel, H. B. *J. Phys. Chem.* **1990**, *94*, 5523.

(30) Huber, K. P.; Herzberg, G. *Molecular Spectra and Molecular Structure, Vol. III. Electronic Spectra and Electronic Structure of Polyatomic Molecules*; Van Nostrand: New York, 1979.